Catalysts **2012**, *2*, 352-367; doi:10.3390/catal2030352

OPEN ACCESS

catalysts

ISSN 2073-4344

www.mdpi.com/journal/catalysts

Article

Alumina-Supported Manganese Catalysts for Soot Combustion Prepared by Thermal Decomposition of $KMnO_4$

Maria-Eugenia Becerra [1,2], Nayda-Patricia Arias [2,3], Oscar-Hernan Giraldo [2,4], Franz-Edwin López-Suárez [5], Maria-Jose Illán-Gómez [5] and Agustin Bueno-López [5,*]

1 Department of Chemistry, Caldas University, Calle 65 N° 26-10, Manizales, Colombia; E-Mail: maria.becerra@ucaldas.edu.co

2 Laboratory of nanostructured and functional materials, National University of Universidad in Manizales, Carrera 27 N° 64-60, Manizales, Colombia; E-Mails: npariasd@gmail.com (N.-P.A.); ohgiraldoo@unal.edu.co (O.-H.G.)

3 Department of electric, electronic and computation, Faculty of engineering, National University of Universidad in Manizales, Carrera 27 N° 64-60, Manizales, Colombia

4 Department of Fisics and Chemistry, National University of Universidad in Manizales, Carrera 27 N° 64-60, Manizales, Colombia

5 Department of Inorganic Chemistry, University of Alicante, Carretera San Vicente del Raspeig s/n-03690, Alicante 03080, Spain; E-Mails: franz.lopez@ua.es (F.-E.L.-S.); illan@ua.es (M.-J.I.-G.)

* Author to whom correspondence should be addressed; E-Mail: agus@ua.es; Tel.: +34-600-948-665; Fax: +34-965-903-454.

Received: 23 July 2012; in revised form: 13 August 2012 / Accepted: 16 August 2012 / Published: 11 September 2012

Abstract: Alumina-supported manganese catalysts with cryptomelane and/or birnessite structure have been prepared using a simple method based on the thermal decomposition of potassium permanganate. The samples have been characterized by XRD, FTIR, TGA, DSC, N_2 adsorption at −196 °C, SEM, H_2-TPR and XPS, and their catalytic activity for soot combustion has been tested and compared to that of a reference Pt/alumina catalyst. The thermal decomposition of alumina-supported $KMnO_4$ yields a mixture of supported birnessite and potassium manganate which is the most effective, among those prepared, to lower the soot combustion temperature. However, this material is not useful for soot combustion because the accelerating effect is not based on a catalytic process but on the oxidation of soot by potassium manganate. A suitable soot combustion catalyst is obtained after potassium manganate is removed by water washing, yielding only the birnessite phase

on the γ-Al_2O_3 support. This birnessite phase can be transformed into cryptomelane by calcination at 600 °C. These two samples, γ-Al_2O_3-supported birnessite and cryptomelane are suitable catalysts for soot combustion in NO_x/O_2 mixtures, as their catalytic activity is based on the NO_2-assited mechanism, that is, both catalysts accelerate the oxidation of NO to NO_2 and NO_2 promotes soot oxidation. The soot combustion temperatures obtained with these birnessite/cryptomelane alumina-supported catalysts are similar to that obtained with the reference Pt/alumina catalyst.

Keywords: soot; manganese catalyst; supported catalyst; NO*x*; birnessite; cryptomelane

1. Introduction

One of the main problems related with the development of the XXI century society is environmental pollution; the emission of nano/micro particles of carbon (soot) by diesel-engines being one of the unsolved issues to overcome.

Diesel Particulate Filters (DPFs) are able to remove soot from exhaust gas, and these filters must be continuously or periodically regenerated by thermal or catalytic combustion of the soot collected [1]. Among the different catalysts proposed for this application alkali, alkali-earth, transition and rare-earth metals are the most useful [2–13]. The use of transition metal oxide-based catalysts is an alternative to noble metals, and among them, manganese oxides seem to be promising candidates [5,6].

In a previous study [5], manganese catalysts with birnessite and cryptomelane structure were prepared, characterized, and tested as catalysts for soot combustion with NO_x/O_2. The activity of these catalysts was compared to that of some other commercially available pure manganese oxides (MnO, MnO_2, Mn_2O_3, Mn_3O_4, and natural MnO_2) and it was concluded that both birnessite and cryptomelane are more active for soot combustion than the pure oxides tested. In that study, cryptomelane was prepared by the reflux method [14,15] and birnessite was prepared following the method of *Ching et al*. [16]. In a further study [6], manganese oxides with cryptomelane and/or birnessite structure were successfully prepared by a simple method based on the thermal decomposition of potassium permanganate. Their catalytic activity to accelerate soot combustion was confirmed, and it was also concluded that the catalytic combustion of soot occurs by the NO_2-assisted mechanism, which is the most convenient to operate under real conditions.

For the practical use of soot combustion catalysts, the active phases have to be loaded in a proper substrate. A typical DOC (Diesel Oxidation Catalyst) used in a CRT (Continuously Regenerating Trap) system for CO and hydrocarbons oxidation, and also to oxidize NO to NO_2, which promotes the combustion of soot collected in a filter placed downstream (NO_2-assisted soot combustion), consists of an inert substrate coated with an alumina layer where different active components (typically containing noble metals) are loaded.

The goal of the current study is to evaluate if alumina-supported manganese catalysts with cryptomelane and/or birnessite structure can be prepared by a simple method based on the thermal decomposition of potassium permanganate [6]. The soot combustion activity of alumina-supported manganese catalysts has been tested and compared with that of a reference Pt/alumina catalyst.

2. Results and Discussion

2.1. Characterization Results

The X-ray diffraction patterns of the manganese-alumina samples prepared are included in Figure 1. In addition, in order to analyze potential changes occurring on the alumina support during the preparation of the supported catalysts, the XRD patterns of the γ-Al_2O_3 support calcined at 400 °C and 600 °C have also been included.

Figure 1. XRD patterns: **(a)** γ-Al_2O_3 calcined at 400 °C; (**b**) γ-Al_2O_3 calcined at 600 °C; (**c**) MnAlT400; (**d**) MnAlT400W and (**e**) MnAlW600.

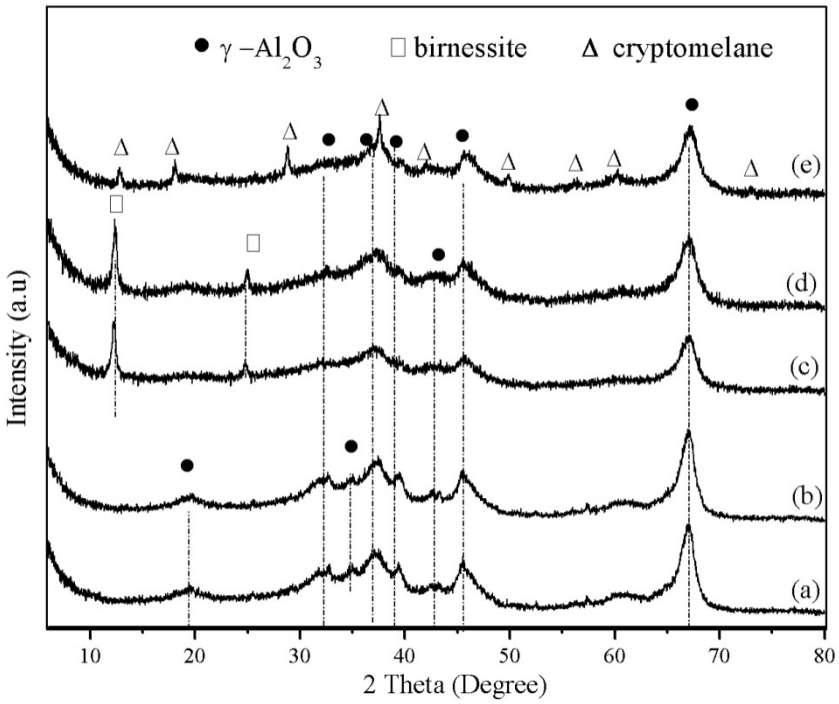

The diffraction peaks of γ-Al_2O_3 appear at 2θ = 19.51°, 32.7°, 37.5°, 39.24°, 45.5° and 67.1°, being consistent with the diffractograms reported for this material (JCPDS: 00-046-1215) [17,18]. The XRD patterns of γ-Al_2O_3 are equal after calcinations at 400 °C and 600 °C, evidencing the thermal stability of this support in the range of temperatures analyzed.

The diffraction patterns of MnAlT400 and MnAlT400W present peaks assigned to the γ-Al_2O_3 support along with peaks at 2θ = 12.54° and 25.10°, which can be attributed to birnessite [19]. The expected peaks of potassium manganate were not detected by XRD in MnAlT400, probably due to its high dispersion on the support. However, the presence of potassium manganate was evidenced in a previous study performed with unsupported manganese samples (without alumina) after calcinations of potassium permanganate at 400 °C [6]. The XRD pattern changes significantly for MnAlW600, showing characteristics peaks of criptomelane (JCPDS 44-0141) [20].

Evidence of the presence of potassium manganate in MnAlT400 are the greenish color of the water used in the washing step performed to MnAlT400 and the increase of the intensity of the birnessite peaks of MnAlT400W with regard to those of MnAlT400. In addition, the K/Mn molar ratio

determined from Atomic Absorption Spectrometer (AAS) analysis values (data in Table 1), is higher in MnAlT400 than in MnAlT400W, that is, decreases after the washing step due to potassium manganate removal. The SEM images included in Figure 2 also support the formation of potassium manganates upon calcination of γ-Al_2O_3-supported $KMnO_4$. γ-Al_2O_3 (Figure 2a) consists of quite spherical particles of 100–200 μm, the difference in contrast between the particles in this figure is assigned to "charging effect" on the surface of particles probably because this material is dielectric and the electrons are accumulated on it. These spherical particles are covered by potassium manganate needles of 15–40 μm length (Figure 2b). These needles are removed by water washing, and therefore, are neither observed in MnAlT400W nor in MnAlW600.

Table 1. Atomic Absorption Spectrometer (AAS) elemental analysis.

Sample	Al (wt%)	Mn (wt%)	K (wt%)	K/Mn (Molar ratio)
MnAlT400	30.3	5.8	3.6	0.87
MnAlT400W	38.2	5.8	1.8	0.44

Figure 2. SEM images: (**a**) γ-Al_2O_3; (**b**) MnAlT400; (**c**) MnAlT400W and (**d**) MnAlW600.

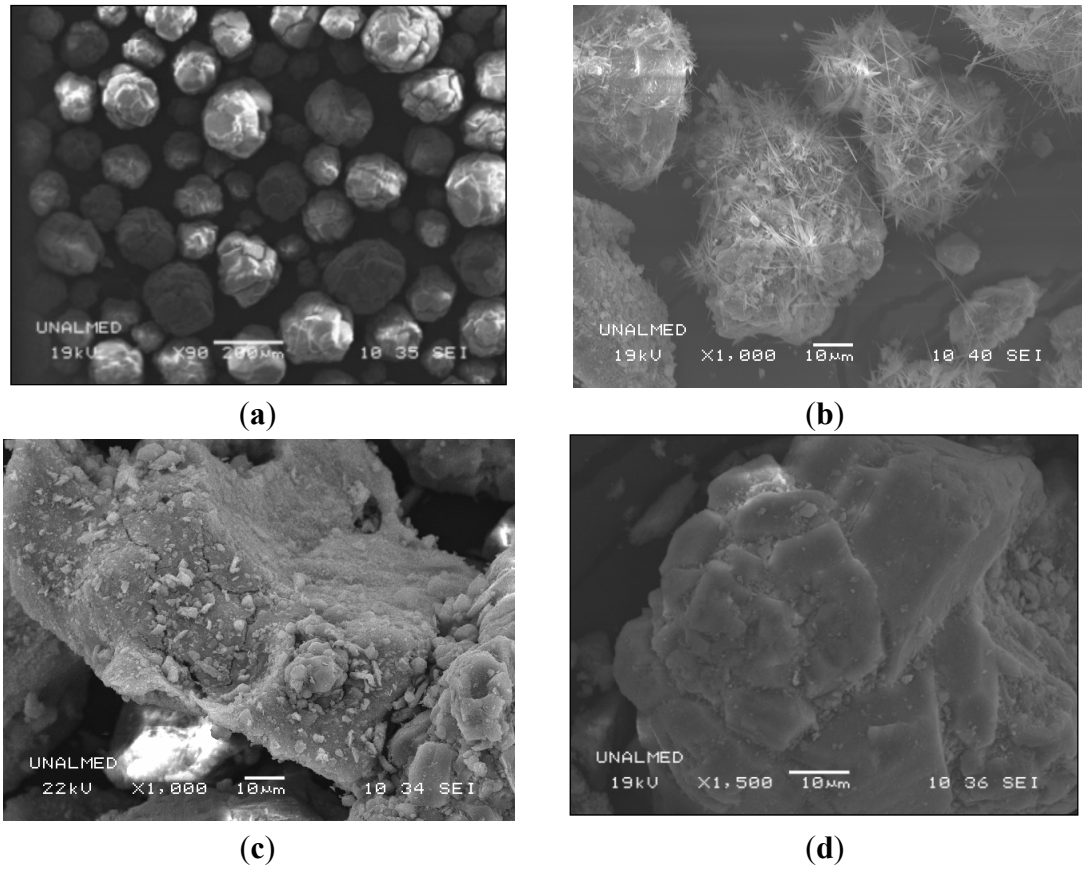

(**a**) (**b**)

(**c**) (**d**)

Figure 3 shows the FTIR spectra of the manganese-alumina samples together with those of the γ-Al_2O_3 support calcined at 400 °C and 600 °C. The bands between 3800–3680 cm^{-1} and 2000–1500 cm^{-1} are assigned to the O-H vibration of adsorbed water and/or to surface hydroxyl groups [21], and those between 980–550 cm^{-1} are attributed to Al-O bond vibrations [22]. The spectra of γ-Al_2O_3 after

calcinations at 400 °C and 600 °C are quite similar to each other, supporting that the γ-Al_2O_3 support is thermally stable in the range of temperatures studied, which is consistent with the XRD conclusions.

Figure 3. FTIR spectra: (**a**) γ-Al_2O_3 calcined at 400 °C; (**b**) γ-Al_2O_3 calcined at 600 °C; (**c**) $KMnO_4$ impregnated on γ-Al_2O_3 (non-calcined); (**d**) MnAlT400; (**e**) MnAlT400W and (**f**) MnAlW600.

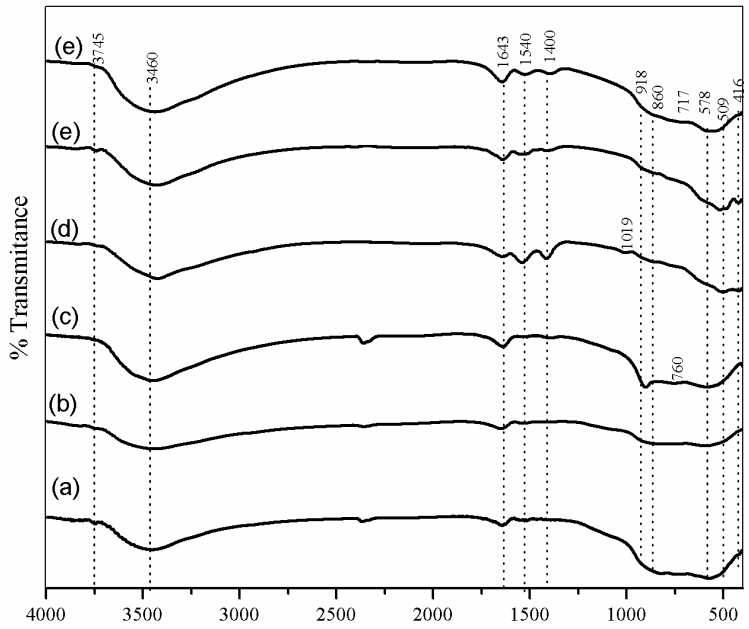

As can be observed in Figure 3, the band at 3745 cm^{-1}, assigned to adsorbed water and/or hydroxyl groups on γ-Al_2O_3, disappear upon $KMnO_4$ impregnation, and the position of those at 3460 and 1643 cm^{-1} shift with respect to their position on bare alumina. The bands at 1400, 918 and 760 cm^{-1} are attributed to $KMnO_4$, and the shift in position of these bands with regard to the typical positions reported for pure $KMnO_4$ [6,23] evidences a certain interaction between $KMnO_4$ and γ-Al_2O_3.

In sample MnAlT400, the IR bands below 700 cm^{-1} are assigned to vibrational modes of Mn-O bonds [24] and the bands at 509 y 422 cm^{-1} are characteristics of birnessite [25]. The band at around 1019 cm^{-1}, which can be ascribed to Mn=O vibrations, suggests the presence of manganate-type oxides (Mn(VI)Ox) [26]. This band disappears after washing the MnAlT400 sample (see IR spectra of MnAlT400W) due to the removal of this soluble specie. After calcinations at 600 °C of the washed sample (see IR spectra of MnAlTW600) a new band appears at 1022 cm^{-1}, which has been reported for the vibration mode of Mn^{3+}–O [27], and finally some studies attribute the bands between 450 and 750 cm^{-1} to the vibration of Mn–O bonds in cryptomelane [28].

Figures 4 and 5 show the TGA and DSC results, respectively, and Table 2 compiles the weight losses determined from TGA profiles for different temperature ranges. The weight losses observed below

250 °C can be partially attributed to water release and the weight losses occurring above 500 °C are associated with structural changes that imply O_2 delivery [6]. For instance, in γ-Al_2O_3-supported $KMnO_4$, the endothermic DSC peaks at temperatures below 200 °C are due to the release of physisorbed water, and the exothermic peaks at 288 °C and 537 °C are associated to phase transitions occurring with oxygen release.

Figure 4. TGA profiles (obtained under nitrogen atmosphere): (**a**) γ-Al_2O_3; (**b**) $KMnO_4$ impregnated on γ-Al_2O_3 (non-calcined); (**c**) MnAlT400; (**d**) MnAlT400W y; (**e**) MnAlW600.

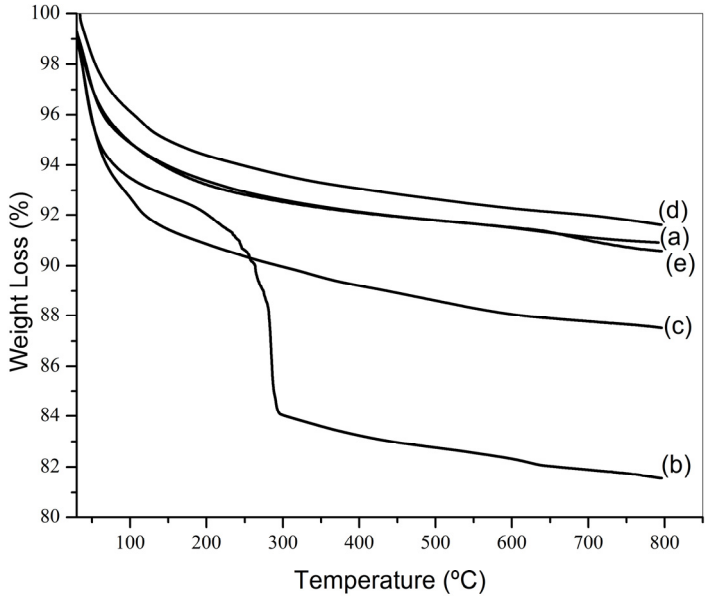

Figure 5. DSC profiles: (**a**) $KMnO_4$ impregnated on γ-Al_2O_3 (non-calcined); (**b**) MnAlT400 and (**c**) MnAlT400W.

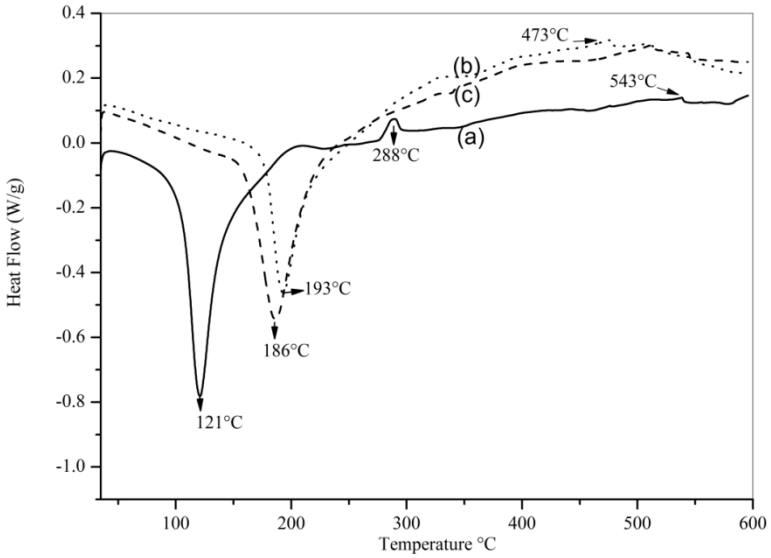

Table 2. Weight loss in TGA experiments in N_2 atmosphere.

Sample	Until 250 °C (wt%)	250 to 500 °C (wt%)	Above 500 °C (wt%)	Total (wt%)
γ-Al_2O_3	7.2	1.0	0.9	9.1
$KMnO_4$ impregnated on γ-Al_2O_3 (non-calcined)	9.5	7.8	1.2	18.5
MnAlT400	9.7	1.7	1.1	12.5
MnAl T400W	6.5	0.9	1.0	8.4
MnAlW600	7.2	1.0	1.2	9.4

The weight loss suffered by γ-Al_2O_3-supported $KMnO_4$ between 250 and 500 °C is related to the decomposition of $KMnO_4$, considering that the γ-Al_2O_3 support is stable in the range of temperatures studied, as deduced from XRD and FTIR. This $KMnO_4$ decomposition is in accordance with previously reported DSC results [6].

The quantitative weight loss values included in Table 2 show that the weight loss suffered until 250 °C by the washed sample (MnAlT400W) is lower than that suffered by the counterpart non-washed sample (MnAlT400), which is attributed to the hygroscopic character of manganates, as it was reported by Kappenstein *et al*. [29]. The weight loss of MnAlW600 below 250 °C is due to the release of water adsorbed in the porous structure of cryptomelane. The structural changes related with the formation of manganese oxide phases, as determined by XRD and FTIR, are in accordance with the DSC profiles (Figure 5).

In conclusion, the TGA results discussed are consistent with those previously obtained with pure $KMnO_4$ (without alumina) [6]. Birnessite and potassium manganate are formed after $KMnO_4$ calcination at 400 °C, and transformation to cryptomelane occurs after potassium manganate removal by water washing and calcination at 600 °C.

N_2 adsorption–desorption isotherms are shown in Figure 6, and different parameters obtained from these isotherms are compiled in Table 3. All samples present type IV isotherms, according to IUPAC classification [30], with considerable N_2 adsorption at low relative pressures, which is indicative of microporosity [31], and hysteresis cycles. These profiles indicate that the materials present also a mesoporous structure and them shown capillary condensation above P/Po 0.3. According to the De Boer [30–32] classification, the hysteresis cycles present contributions of slit–shaped pores (B) and interconnected pores with bottleneck shape (E). The mesopores size distributions determined by the BJH method (inset in Figure 6) show peaks centered between 35.98 Å and 37.86 Å, without significant change among samples.

Figure 6. N_2 adsorption–desorption isotherms: (**a**) γ-Al_2O_3; (**b**) MnAlT400; (**c**) MnAlT400W; (**d**) MnAlW600 (Inset, mesoporous size distribution obtained by BHJ method).

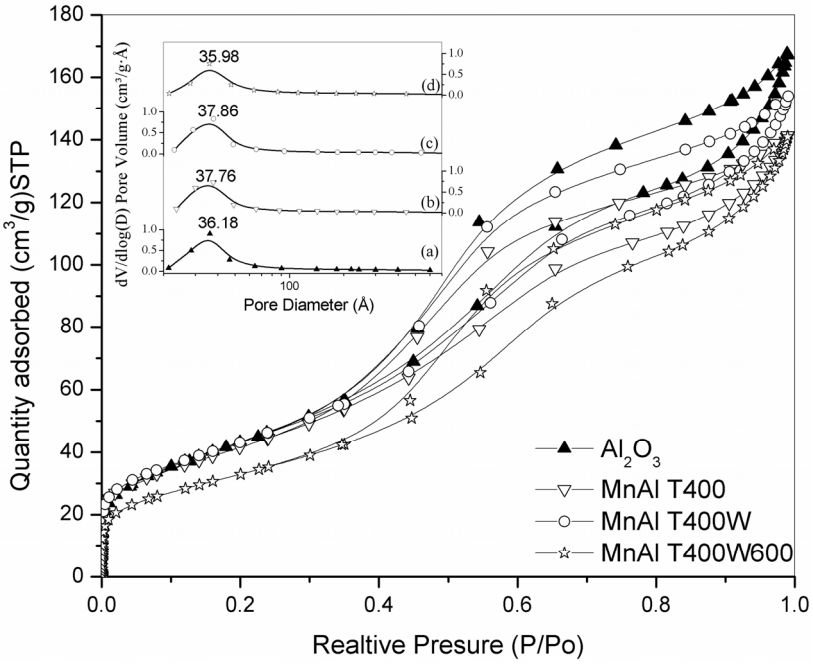

Table 3. Brunauer-Emmet-Teller (BET) area, pore volume (V_{pore}) and average pore diameter (D_{BJH}).

Material	S_{BET} (m^2/g)	V_{pore} (cm^3/g)	D_{BJH} (Å)
γ-Al_2O_3	165	0.26	41.2
$KMnO_4$ impregnated on γ-Al_2O_3 (non-calcined)	148	0.20	36.8
MnAlT400	151	0.22	41.2
MnAlT400W	158	0.25	41.4
MnAlT400W600	121	0.22	44.7

The micropore size distribution, obtained by the HK method, (Figure 7) is monomodal for MnAlT400, while bimodal for bare γ-Al_2O_3, MnAlT400W and MnAlW600, suggesting the presence of primary and secondary micropores [33]. These results evidence that potassium manganate on MnAlT400 blocks part of the γ-Al_2O_3 microporosity, in agreement with results reported by other authors [34], and the closed micropores becomes again open after removal of the soluble salts by water washing. The BET surface areas included in Table 3 are consistent with this conclusion. The BET surface area of γ-Al_2O_3 decreases after $KMnO_4$ impregnation, and increases again after the washing step (sample MnAlT400W).

Figure 7. Micropore size distribution (obtained by HK method): (**a**) γ-Al_2O_3; (**b**) MnAlT400; (**c**) MnAlT400W and (**d**) MnAlW600.

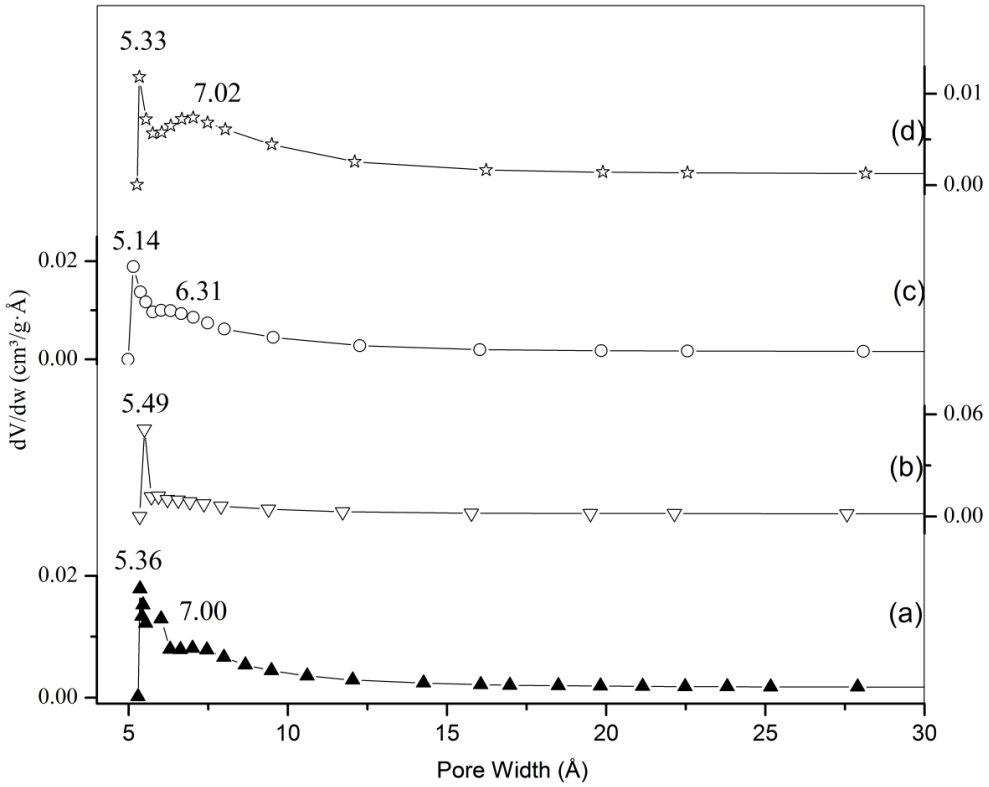

H_2 reduction profiles for all samples prepared are included in Figure 8. According with the description of several authors [35–37], the reduction of supported manganese (IV) oxide occurs in several consecutive steps. The lower temperature peaks are attributed to the reduction of Mn^{4+} to Mn_3O_4 following the reactions sequence: $MnO_2 \rightarrow Mn_2O_3 \rightarrow Mn_3O_4$. The reduction step taking place at higher temperatures is attributed to Mn_3O_4 reduction to MnO.

Figure 8. Samples characterization by H_2-TPR.

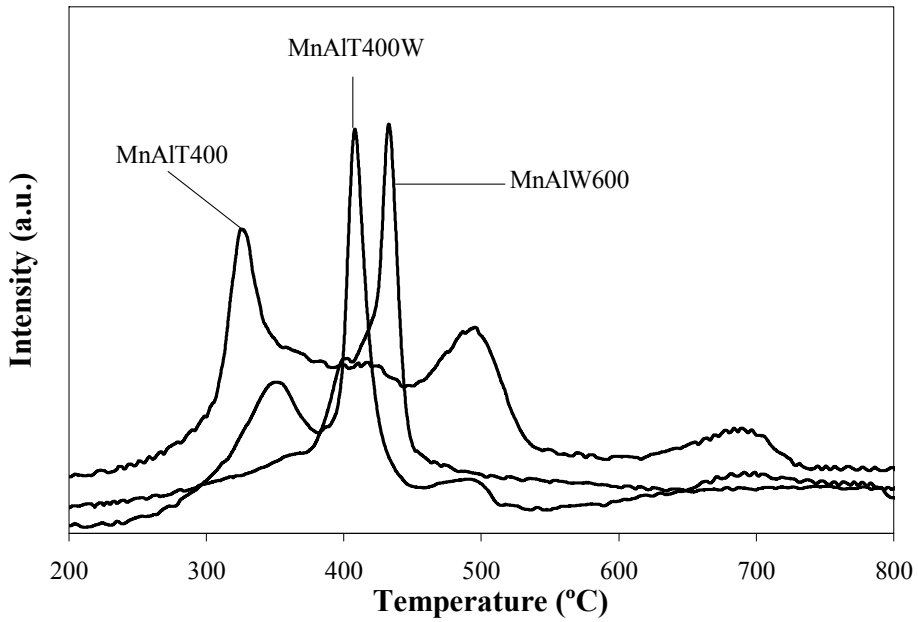

The H_2 reduction profile obtained with MnAlW600 shows two main reduction peaks at 400 °C and 434 °C, which could indicate that the reduction proceeds following the sequence of steps KMn_8O_{16} (cryptomelane)→Mn_3O_4→MnO. A similar H_2 reduction profile is obtained with MnAlT400W, but the temperatures of the main peaks are shifted to lower temperatures. The intensity of the second peak is always higher than that of the first one in both samples. On the contrary, the H_2 reduction profile of MnAlT400 (non-washed sample) differs from those of the washed samples (MnAlW600 and MnAlT400W) due to the presence of salts with manganese cations in oxidation states higher than +4. In conclusion, the H_2 reduction experiments suggest the presence of Mn cations with oxidation state near +4, as expected for birnessite and cryptomelane.

XPS characterization was used in order to obtain additional information about the oxidation state of manganese on the different samples by using a method reported elsewhere [6]. Figure 9 plots the formal oxidation state of manganese for three different commercial manganese oxides (MnO, Mn_3O_4 and MnO_2, by Aldrich) with regard to the difference between the binding energy of the Mn $2p^{3/2}$ and Mn $2p^{1/2}$ peaks measured experimentally by XPS with each oxide (+2, +2.7 and +4, respectively). These reference values allow us to drawn a calibration line, and thus, the formal oxidation state of manganese in MnAlT400, MnAlT400W and MnAlW600 can be estimated by introducing in this trend line the XPS values calculated by difference between the corresponding binding energies of the Mn $2p^{3/2}$ and Mn $2p^{1/2}$ transitions. The formal oxidation states estimated are +4.3, +3.5 and +3.7 for MnAlT400, MnAlT400W and MnAlW600, respectively. The value obtained with the unwashed sample (MnAlT400; +4.3) is slightly above +4, which is consistent with the presence of manganate salts (in addition to birnessite) where the oxidation state of manganese is +6. The values obtained with the washed samples are between +3 and +4 because the manganates have been removed and only the birnessite and/or cryptomelane phases remain on the samples. As expected, the formal oxidation state obtained with the sample calcined at 600 °C (MnAlW600; +3.7) is slightly higher to that obtained with the sample calcined at 400 °C (MnAlW600; +3.5). These XPS results are in agreement with the

H_2-TPR conclusions and confirm the presence of manganese cations with the oxidation states expected for birnessite and cryptomelane phases, which are the phases identified by XRD and FTIR.

Figure 9. Formal oxidation state of manganese as a function of the difference between the binding energy of the Mn $2p^{3/2}$ and Mn $2p^{1/2}$ XPS peaks.

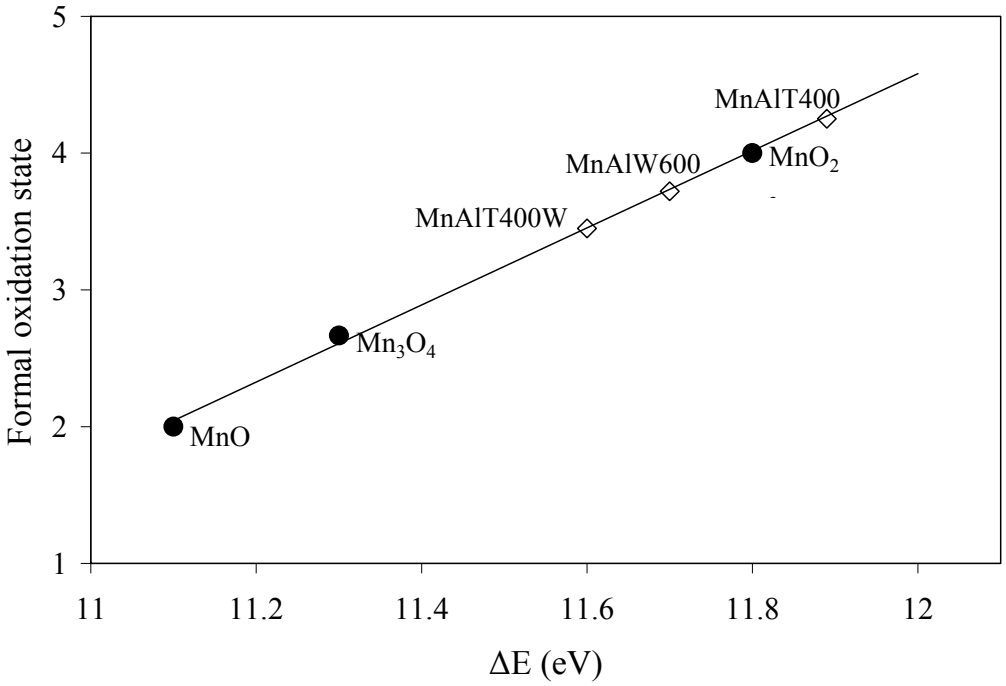

2.2. Catalytic Tests

The catalytic combustion of soot was evaluated in O_2/N_2 and $NO_x/O_2/N_2$. The soot conversion profiles obtained in O_2/N_2, and included in Figure 10, show that only the sample MnAlT400 is able to lower the soot combustion temperature with regard to the uncatalyzed reaction in these reactions conditions. This is attributed to the presence of potassium manganates, that is, this is not a catalytic effect but a redox reaction where potassium manganate oxidises soot.

In experiments performed in $NO_x/O_2/N_2$ (Figure 11), the lowest soot combustion temperature is also achieved with MnAlT400. However, in the presence of NO_x, the washed samples (MnAlW600 and MnAlT400W) are also able to lower the soot combustion temperature with respect to the uncatalyzed reaction. These results are consistent with those previously obtained with unsupported manganese samples of similar composition. In the previous study [6], it was concluded that the combustion of soot assisted by birnessite and cryptomelane catalysts (once manganese salts have been removed) occurs by the NO_2 mechanism, that is, by acceleration of the NO oxidation to NO_2, which is much more oxidizing than NO and O_2. For comparison, the soot combustion profile obtained with a Pt/Al_2O_3 reference catalyst has been included in Figure 11. Note, that the onset of the soot combustion temperatures obtained with the manganese samples are not very different to that obtained with Pt. Therefore, these oxides are able to accelerate soot combustion and would be a valuable alternative for catalytic combustion of soot, since they are cheaper than Pt catalysts and easy to prepare.

Figure 10. Soot conversion profiles in catalytic tests performed in O_2/N_2.

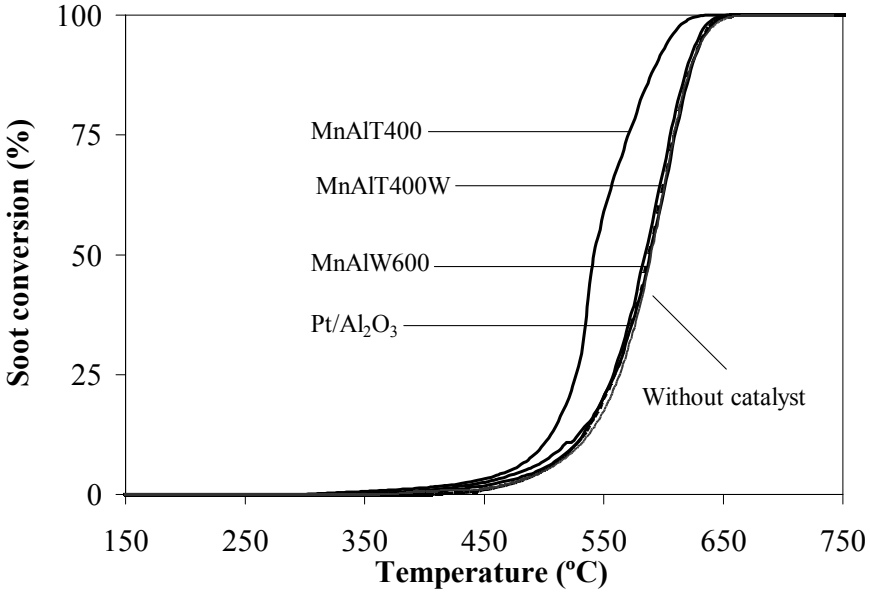

Figure 11. Soot conversion profiles in catalytic tests performed in NO_x/O_2.

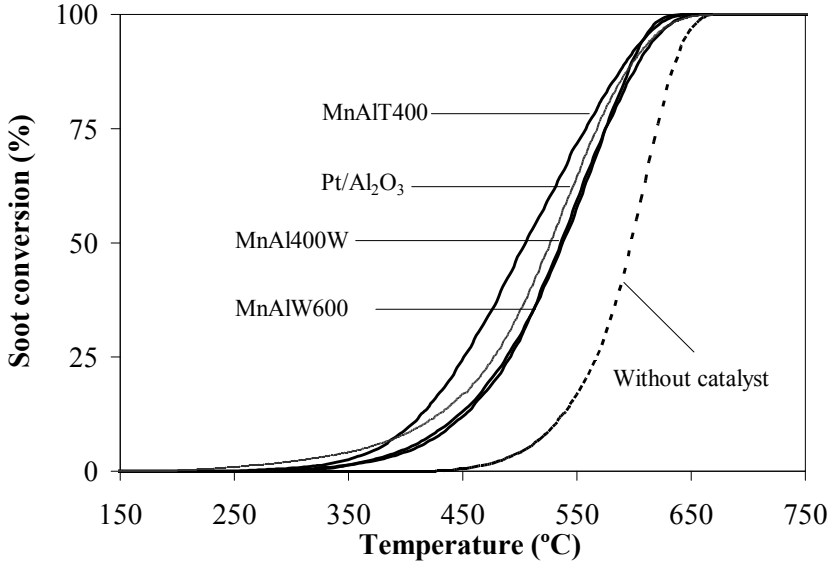

In order to analyze in more detail the reaction mechanism by which these alumina-supported manganese catalysts (MnAlW600 and MnAlT400W) accelerate soot combustion in a NO_x/O_2 gas mixtures, blank experiments (only with the catalysts and without soot) have been performed with the $NO_x/O_2/N_2$ gas mixture. The NO_2 percentage (produced by NO oxidation) in total NO_x basis is plotted in Figure 12 as a function of temperature. These results confirm that the manganese catalysts prepared in this study are able to oxidize NO to NO_2, and the amount of NO_2 yielded is not very different to that produced by the Pt/Al_2O_3 reference catalyst (the amounts of NO_2 evolved are reported in Figure 12 in mmol/gr). These blank experiments confirm that the catalyzed combustion of soot takes place with the participation of the NO_2-assisted mechanism.

Figure 12. NO_2 percentage in blank experiments (without soot) performed in NO_x/O_2. The amounts of NO_2 evolved are reported between parentheses in mmol/gr).

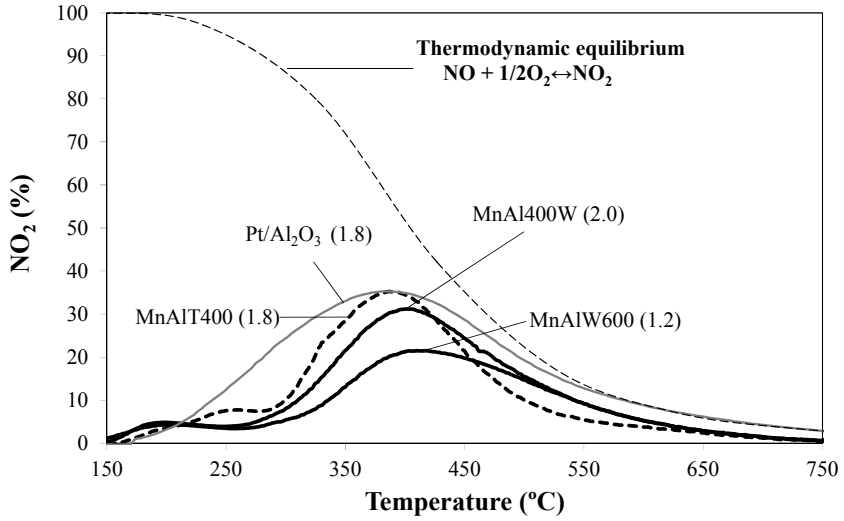

3. Experimental Section

3.1. Preparation of Sample

Alumina-supported manganese samples were synthesized by means of the wet impregnation method [38]. γ-Al_2O_3 (Carlo Erba) was impregnated with Commercial $KMnO_4$ (J.T. Baker, analytical grade) in solution and the solvent was removed at 90 °C. The nominal MnO_4^- loading was 4.5 wt%.

Three alumina-supported manganese samples, referred to as MnAlT400, MnAlT400W and MnAlW600, were prepared following different procedures:

- MnAlT400: After $KMnO_4$ impregnation on γ-Al_2O_3, the sample is calcined in air at 400 °C for 6 h (heating rate 10 °C/min).
- MnAlT400W: The previously prepared sample MnAlT400 is washed with distilled and deionized water to remove soluble salts (potassium manganate), and after washing, the sample is dried at 60 °C for 24 h.
- MnAlW600: The previously prepared sample MnAlT400W is calcined at 600 °C for 6 h (heating rate 10 °C/min).

In addition, a 1% Pt/γ-Al_2O_3 catalyst was prepared by excess-volume impregnation of γ-Al_2O_3 using $Pt(NH_3)_4(NO_3)_2$ as precursor. After impregnation, the catalyst is heated in static air at 110 °C for 12 h and calcined at 700 °C for 5 h.

3.2. Characterization of Samples

The samples were characterised using the same techniques and the technical specifications reported by Becerra *et al.* [6] in brief: (i) Powder X-ray diffraction patterns were obtained in a Rigaku MiniFlex II diffractometer; (ii) infrared measurements were carried out using a NICOLET 380 spectrometer with a DTGS detector; (iii) thermogravimetric analysis (TGA) was performed in a thermo balance, by TA

Instruments, model TGA Q500 and (iv) differential scanning calorimetric measurements were performed with a TA Instruments equipment, model DSC Q100.

Elemental analysis was performed in an Atomic Absorption Spectrometer (AAS) Perkin Elmer, model 3110. For this purpose, the samples were dissolved (even the alumina support) by a fusion process with lithium metaborate [39]. 50 mg of sample are mixed with 300 mg of lithium metaborate and calcined at 1000 °C for 15 min. The mixture is cooled down to room temperature, and 20 mL of distilled and deionized water and 5 mL of 37% HCl are added. This solution is heated until boiling under continuous stirring, and once the solids are dissolved, 1 mL of 15% lanthanum chloride is added. Finally, the solution is diluted with water for elemental analysis. The Mn and K contents were determined at wavelengths of 279.5 nm and 766.5 nm, respectively.

Scanning Electron Microscopy (SEM) images were recorded with a Jeol JSM 5910LV microscope, operated at 15 kV and 19 kV in high vacuum mode, with Back-Scattered Electrons (BES) and secondary electron imaging (SEI) for image generation.

N_2 adsorption-desorption isotherms were measured at −196 °C in a volumetric set up (Micromeritics, model ASAP 2020). The specific surface area was calculated by the Brunauer-Emmet-Teller (BET) method and porous distribution by Joyner-Hallenda (BJH) and Hovarth-Kawazoe (HK) methods.

XPS analysis was carried out in a VG-Microtech Multilab electron spectrometer using Mg-Kα (1253.6 eV) radiation source. H_2-TPR experiments were performed in a Micromeritics device; model Pulse ChemiSorb 2705, with a TCD detector.

3.3. Catalytic Tests

Catalytic tests were performed in a fixed-bed reactor at atmospheric pressure under a gas flow (500 mL/min) containing 5% O_2 balanced with N_2 or 500 ppm NO_x + 5% O_2 balanced with N_2. The model soot used was a carbon black from Degussa S.A. (Printex-U). The experiments consisted of heating the soot-catalyst mixtures from 25 to 750 °C at 10 °C/min. The soot-catalyst mixtures contained 80 mg of catalyst + 20 mg of soot + 300 mg SiC, and were prepared with a spatula following the so-called "*loose contact*" procedure [40]. Blank experiments were performed only with the catalysts (without soot) under similar experimental conditions. The gas composition was monitored by specific NDIR-UV (Non Dispersive Infrared Ultra-Violet) gas analyzers for NO, NO_2, CO, CO_2 and O_2 and the soot conversion was determined from CO and CO_2 evolved.

4. Conclusions

From the results presented and discussed in this paper, it can be concluded that different alumina-supported manganese oxide catalysts have been obtained by impregnation of potassium permanganate on γ-Al_2O_3 and subsequent thermal decomposition. Some of the prepared materials can be considered for the regeneration of DPF filters since they are able to catalytically accelerate the soot combustion process.

Thermal decomposition of alumina-supported potassium permanganate yields a mixture of supported birnessite and potassium manganate. This material is the most effective, among those prepared to lower the soot combustion temperature, but has no practical relevance for soot combustion because the accelerating effect is based on a redox process thus consuming the raw samples. A suitable

soot combustion catalyst is obtained after potassium manganate removal by water washing, only leaving the birnessite phase on the γ-Al_2O_3 support. The birnessite phase can then be transformed into cryptomelane by calcinations at 600 °C.

The γ-Al_2O_3-supported birnessite and cryptomelane samples are suitable catalysts for soot combustion in NO_x/O_2 mixtures, and their catalytic activity is based on the NO_2-assisted mechanism, that is, both catalysts accelerate the oxidation of NO to NO_2 which promotes soot oxidation.

Acknowledgments

The authors thank to Spanish government (MICINN project CTQ2009-07475), DIMA (Dirección de Investigaciones) and Laboratorio de Magnetismo y Materiales Avanzados (Universidad Nacional de Colombia, Sede Manizales) and Vicerrectoría de Investigaciones de la Universidad de Caldas for the financial support.

Conflict of Interest

The authors declare no conflict of interest.

References

1. Setten, B.A.A.L.; Makkee, M.; Moulijn, J.A. Science and technology of catalytic diesel particulate filters. *Catal. Rev*. **2001**, *43*, 489–564.
2. Bueno-López, A.; Soriano-Mora, J.M.; García-García, A. Study of the temperature window for the selective reduction of NO_x in O_2-rich gas mixtures by metal-loaded carbon. *Catal. Commun*. **2006**, *7*, 678–684.
3. López-Suárez, F.E.; Bueno-López, A.; Illán-Gómez, M.J. Cu/Al_2O_3 catalysts for soot oxidation: Copper loading effect. *Appl. Catal.* **2008**, *84*, 651–658.
4. López-Suárez, F.E.; Bueno-López, A.; Illán-Gómez, M.J.; Ura, B.; Trawczynski, J. Potassium stability in soot combustion perovskite catalysts. *Top. Catal*. **2009**, *55*, 2097–2100.
5. Atribak, I.; Bueno-Lopez, A.; García-García, A.; Navarro, P.; Frías, D.; Montes, M. Catalytic activity for soot combustion of birnessite and cryptomelane. *Appl. Catal*. **2010**, *93*, 267–273.
6. Becerra, M.E.; Arias, N.P.; Giraldo, O.H.; López Suárez, F.E.; Illán Gómez, M.J.; Bueno López, A. Soot combustion manganese catalysts prepared by thermal decomposition of $KMnO_4$. *Appl. Catal.* **2011**, *102*, 260–266.
7. Ciambelli, P.; Palma, V.; Russo, P.; Vaccaro, S.J. Redox properties of a TiO_2 supported Cu-V-K-Cl catalyst in low temperature soot oxidation. *J. Mol. Catal.* **2003**, *204–205*, 673–681.
8. Harrison, P.G.; Ball, I.K.; Daniell, W.; Lukinskas, P.; Caspedes, M.E.; Mirò, E.; Ulla, M.A. Cobalt catalysts for the oxidation of diesel soot particulate. *Chem. Eng. J.* **2003**, *95*, 47–55.
9. Russo, N.; Furfori, S.; Fino, D.; Saracco, G.; Specchia, V. Lanthanum cobaltite catalysts for diesel soot combustion. *Appl. Catal.* **2008**, *83*, 85–95.
10. Peralta, M.A.; Gross, M.S.; Ulla, M.A.; Querini, C.A. Catalyst formulation to avoid reaction runaway during diesel soot combustion. *Appl. Catal.* **2009**, *367*, 59–69.

11. Aneggi, E.; Llorca, J.; de Leitenburg, C.; Dolcetti, G.; Trovarelli, A. Soot combustion over silver-supported catalysts. *Appl. Catal.* **2009**, *91*, 489–498.
12. Wu, X.; Lin, F.; Xu, H.; Weng, D. Effects of adsorbed and gaseous NOx species on catalytic oxidation of diesel soot with MnO_x-CeO_2 mixed oxides. *Appl. Catal.* **2010**, *96*, 101–109.
13. Liu, J.; Zhao, Z.; Xu, C.; Duan, A.; Jiang, G. Simultaneous Removal of Soot and NO_x over the $(La_{1.7}Rb_{0.3}CuO_4)_x$/nm CeO_2 Nanocomposite Catalysts. *Ind. Eng. Chem. Res*. **2010**, *49*, 3112–3119.
14. Luo, J.; Zhang, Q.; Huang, A.; Suib, S.L. Total oxidation of volatile organic compounds with hydrophobic cryptomelane-type octahedral molecular sieves. *Microporous Mesoporous Mater*. **2000**, *35*, 209–216.
15. Shen, Y.F.; Zerger, R.P.; DeGuzman, R.N.; Suib, S.L.; McCurdy, L.; Potter, D.I. Octahedral molecular sieves: Synthesis, characterization and applications. *Science* **1993**, *260*, 511–515.
16. Ching, S.; Landrigan, J.A.; Jorgensen, M.L.; Duan, N.G.; Suib, S.L.; O'Young, C.L. Sol-Gel synthesis of birnessite from $KMnO_4$ and simple sugars. *Chem. Mater*. **1995**, *7*, 1604–1606.
17. International Centre for Diffraction Data (ICDD). *Powder Diffraction Database PDF-2*; International Centre for Diffraction Data: Newton Square, PA, 2003; Set 53.
18. Klose, F.; Wolff, T.; Lorenz, H.; Seidel-Morgenstern, A.; Suchorski, Y.; Piórkowska, M.; Weiss, H. Active species on γ-alumina-supported vanadia catalysts: Nature and reducibility. *J. Catal*. **2007**, *247*, 176–193.
19. Drits, V.A.; Silvester, E.; Gorshkov, A.I.; Manceau, A. The structure of synthetic monoclinic Na-rich birnessite and hexagonal birnessite. I. Results from X-ray diffraction and selected area electron diffraction. *Am. Mineral*. **1997**, *82*, 946–961.
20. Tang, Q.; Huang, X.; Wu, C.; Zhao, P.; Chen, Y.; Yang, Y. Structure and catalytic properties of K-doped manganese oxide supported on alumina. *J. Mol. Catal. Chem.* **2009**, *306*, 48–53.
21. Stoilova, D.G.; Nickolov, R.N.; Cheshkova, K.T. Surface and texture characterization of alumina-supported copper and mixed copper–manganese oxide catalysts and their formate precursors. *J. Colloid. Interface Sci*. **2000**, *228*, 24–31.
22. Tejedor-Tejedor, M.I.; Anderson, M.A. The protonation of phosphate on the surface of goethite as studied by CIR-FTIR and electrophoretic mobility. *Langmuir* **1990**, *6*, 602–611.
23. Nakamoto, K. *Infrared and Raman Spectra of Inorganic and Coordination Compounds. Part A: Theory and Applications in Inorganic Chemistry*, 5th ed.; John Wiley and Sons: New York, NY, USA, 1997; p. 199.
24. Julien, C.M.; Massot, M.; Poinsignon, C. Lattice vibrations of manganese oxides: Part I. Periodic structures. *Spectrochim. Acta Mol. Biomol. Spectrosc*. **2004**, *60*, 689–700.
25. Luo, J.; Zhang, Q.; Suib, S.L. Mechanistic and kinetic studies of crystallization of birnessite. *Inorg. Chem*. **2000**, *39*, 741–747.
26. Ali, A.A.; Al-Sagheer, F.A.; Zaki, M.I. Surface texture, morphology and chemical composition of hydrothermally synthesized tunnel-structured manganese (IV) oxide. *Int. J. Inorg. Mater*. **2001**, *3*, 427–435.
27. Gao, T.; Glerup, M.; Krumeich, F.; Nesper, R.; Fjellvåg, H.; Norby, P. Microstructures and spectroscopic properties of cryptomelane-type manganese dioxide nanofibers. *J. Phys. Chem.* **2008**, *112*, 13134–13140.

28. Boxun, H.; Hu, Y.C.; Samuel, J.; Frueh, L.J.; Raymond, J.; Steven, L.S. Removal of aqueous phenol by adsorption and oxidation with doped hydrophobic cryptomelane-type manganese oxide (K-OMS-2) nanofibers. *J. Phys. Chem.* **2010**, *114*, 21.
29. Kappenstein, C.; Pirault-Roy, L.; Guérin, M.; Wahdan, T.; Ali, A.A.; Al-Sagheer, F.A.; Zaki, M.I. Monopropellant decomposition catalysts: V. Thermal decomposition and reduction of permanganates as models for the preparation of supported MnO_x catalysts. *Appl. Catal. Gen*. **2002**, *234*, 145–153.
30. Sing, K.S.W.; Everett, D.H.; Haul, R.A.W.; Moscou, L.; Pierotti, R.A.; Rouquerol, J.; Siemieniewska, T. Reporting Physisorption data for gas/solid systems with special reference to the determination of surface area and porosity. *Pure Appl. Chem*. **1985**, *57*, 603–619.
31. Steven, L.; Suib, S.L. Porous manganese oxide octahedral molecular sieves and octahedral layered materials. *Acc. Chem. Res*. **2008**, *41*, 479–487.
32. De Boer, J.H. *The Structure and Properties of Porous Materials*; Everett, D.H., Stone, F.S., Eds.; Colston Papers: London, UK, 1958; pp. 10–95.
33. Gauden, P.A.; Terzyk, A.P.; Jaroniec, M.; Kowalczyk, P. Bimodal pore size distributions for carbons: Experimental results and computational studies. *Colloid. Interface Sci*. **2007**, *310*, 205–216.
34. Aguero, F.N.; Barbero, P.; Cadus, L.E. Combustion of volatile organic compounds over supported manganese oxide: Influence of the support, the precursor and the manganese loading. *Catal. Today* **2008**, *133*, 493–501.
35. Álvarez-Galván, M.C.; Pawelec, B.; de la Peña O'Shea, V.A.; Fierro, J.L.G.; Arias, P.L. Formaldehyde/methanol combustion on alumina-supported manganese-palladium oxide catalyst. *Appl. Catal.* **2004**, *51*, 83–91.
36. Santos, V.P.; Pereira, M.F.R.; Órfão, J.J.M.; Figueiredo, J.L. The role of lattice oxygen on the activity of manganese oxides towards the oxidation of volatile organic compounds. *Appl. Catal.* **2010**, *99*, 353–363.
37. Gandia, L.M.; Vicente, M.A.; Gil, A. Preparation and characterization of manganese oxide catalysts supported on alumina and zirconia-pillared clays. *Appl. Catal.* **2000**, *196*, 281–292.
38. Perego, C.; Villa, P. Catalyst preparation methods. *Catal. Today* **1997**, *34*, 281–305.
39. *Analytical Methods for Atomic Absorption Spectroscopy*;The Perkin Elmer Corporation: Norwalk, CT, USA, 1994.
40. Neeft, J.P.A.; van Pruissen, O.P.; Makkee, M.; Moulijn, J.A. Catalysts for the oxidation of soot from diesel exhaust gases II. Contact between soot and catalyst under practical conditions. *Appl. Catal.* **1997**, *12*, 21–31.